



MOX–Report No. 48/2013

**An effective algorithm for the generation of  
patient-specific Purkinje networks in computational  
electrocardiology**

SIMONE PALAMARA, CHRISTIAN VERGARA, ELENA  
FAGGIANO, FABIO NOBILE

MOX, Dipartimento di Matematica “F. Brioschi”  
Politecnico di Milano, Via Bonardi 9 - 20133 Milano (Italy)

[mox@mate.polimi.it](mailto:mox@mate.polimi.it)

<http://mox.polimi.it>



# An effective algorithm for the generation of patient-specific Purkinje networks in computational electrocardiology

Simone Palamara<sup>1</sup>, Christian Vergara<sup>2</sup>, Elena Faggiano<sup>1,3</sup>, Fabio Nobile<sup>4</sup>

October 14, 2013

1 MOX– Modellistica e Calcolo Scientifico  
Dipartimento di Matematica “F. Brioschi”  
Politecnico di Milano  
via Bonardi 9, 20133 Milano, Italy

`simone.palamara@polimi.it`

2 Dipartimento di Ingegneria dell’Informazione e Metodi Matematici  
Università di Bergamo  
via Marconi 5, 24044, Italy

`christian.vergara@unibg.it`

3 LaBS, Dipartimento di Chimica, Materiali e Ingegneria Chimica “Giulio Natta”  
Politecnico di Milano

Piazza Leonardo da Vinci 32, 20133 Milano, Italy `elena.faggiano@polimi.it`

4 CSQI – MATHICSE

École Polytechnique Fédérale de Lausanne

Switzerland `fabio.nobile@epfl.ch`

**Keywords:** Computational electrocardiology, Purkinje fibers, Eikonal equation, measures of activation times.

## Abstract

The Purkinje network is responsible for the fast and coordinated distribution of the electrical impulse in the ventricle that triggers its contraction. Therefore, it is necessary to model its presence to obtain an accurate patient-specific model of the ventricular electrical activation. In this paper, we present an efficient algorithm for the generation of a patient-specific Purkinje network, driven by measures of the electrical activation acquired on the endocardium. The proposed method provides a correction of an initial network, generated by means of a fractal law, and it is based on the solution of Eikonal problems both in the muscle and in the Purkinje network. We present several numerical results both in an ideal geometry with synthetic data and in a real geometry with patient-specific clinical measures. These results highlight an improvement of the accuracy of the

patient-specific Purkinje network with respect to the initial one, also in the cases of a cross-validation test and of noisy data.

## 1 Introduction

The inclusion of the *Purkinje system* in the computational models of the electrical activity of the ventricles is fundamental to obtain accurate and realistic numerical results. Indeed, this system, composed by the Purkinje fibers (PF), provides the electrical signal (the *depolarization wave*) to the ventricular muscle. This allows, in normal conditions, the rapid and coordinate activation of the ventricles [9], and then the correct pumping of the blood flow into the arteries. PF are electrically connected to the ventricular muscle only at certain insertion sites, called Purkinje muscle junctions (PMJ) [15]. From these sites the depolarization wave enters the heart muscle, allowing the ventricular excitation and contraction [2].

Despite the essential function of PF in the coordinated activation of the ventricles, they have been usually neglected in the computational models. This was mainly due to the difficulty in obtaining *in vivo* images of PF from radiological analyses, since they are excessively thin for the current clinical imaging resolution. For this reason, the inclusion of the PF in the computational models has been often obtained by means of surrogate models such as the definition of space-dependent conduction muscular properties [17]. There have been, however, some attempts to incorporate PF in the computational models. In particular, three alternatives have been proposed so far to generate a Purkinje network:

- i) Segmentation from ex-vivo images [4];
- ii) A manual procedure based on anatomical knowledge [21, 3];
- iii) Computational algorithms based on a fractal law [1, 10, 16].

Among the three alternatives described above, only strategy i) allows to recover patient-specific information on the network, provided that ex-vivo images are available, which is not a common situation. The second and the third strategies are driven only by general anatomical information and therefore do not allow to generate patient-specific networks. Nevertheless, strategy iii) is very appealing from the computational point of view, since it can be easily incorporated in an available code for the simulation of the electrical activity of the heart.

In this work, we adapt strategy iii) to make it patient-specific by using clinical measurements of the electrical activation in the ventricle to locate accurately the PMJ. In particular, in this work we consider the case of an electrical propagation in the muscle originated from sources located on the endocardium. This is a very common situation, occurring for example for a normal propagation or for an ischemic case, where the sources are all identified with the PMJ. The proposed method has been already considered in [22] for an application to three

real cases characterized by a normal electrical activity and compared with other strategies proposed so far, obtaining very promising results in terms of accuracy. In this paper we aim at describing in details the proposed method and provide an exhaustive computational study of its accuracy and robustness. To do this we apply our method both to an ideal geometry with virtual data generated by solving a forward problem, and to a real geometry with real patient-specific clinical measures.

The numerical results show that our method is accurate and robust in both the geometries, also when cross-validation tests are performed and when noisy data are considered. In particular, our method always features better performance with respect to the case of a non-patient-specific Purkinje network.

The outline of the work is as follows. In Section 2 we introduce the mathematical models considered for the computation of the activation times in the ventricle and in the Purkinje network. In Section 3 we detail our method for the generation of a patient-specific Purkinje network in the case of endocardial sources. In Section 4 we show several numerical results in an idealized geometry to highlight the accuracy and the robustness of our method. Finally, in Section 5 we show the application of our algorithm to a real case obtained by considering patient specific geometry and measures, and we simulate an ischemic case.

## 1.1 A summary of variables and unknowns

We want here to summarize all the variables and unknowns introduced in the text.

$u_m(\mathbf{x}), u_e(\mathbf{x}), u_p(\mathbf{x})$	Activation times in the myocardium, on the endocardium and in the Purkinje network, respectively;
$\Omega_m, \Omega_e, \Omega_p$	Computational domains representing the myocardium, the endocardium and the Purkinje network, respectively;
$\Gamma_m, \Gamma_e, \Gamma_p$ representing the source terms	Part of the domain where the boundary conditions are applied in the myocardium, endocardium and Purkinje network, respectively;
$V_m, V_e, V_p$	Conduction velocity along the muscular fibers in the myocardium, on the endocardium and in the Purkinje network, respectively;
$D$	Anisotropic tensor accounting for the muscular fibers;
$\mathbf{x}_1, \dots, \mathbf{x}_N$	Coordinates of the points where the measures were acquired;
$T_1, \dots, T_N$	Measured activation times;
$\mathbf{w}_1, \dots, \mathbf{w}_M$	Coordinates of the bases of the leaves;
$\mathbf{y}_1, \dots, \mathbf{y}_M$	Coordinates of the PMJ;
$\tau_1, \dots, \tau_M$	Activation times computed at the PMJ by solving the 1D Eikonal problem in the network;
$t_1, \dots, t_N$	Activation times computed at the measures' points $\mathbf{x}_i$ by solving the Eikonal problem on the endocardium or in the myocardium;

## 2 Modeling the electrical activity

### 2.1 The electrical activation in the ventricular muscle

#### 2.1.1 The anisotropic 3D Eikonal problem

The algorithm for the generation of a patient-specific Purkinje network we are going to describe in Section 3 is based on the computation of the discrepancy between the measured and the computed activation times, defined as the instant at which the potential  $W$  reaches the value  $(W_r + W_p)/2$ , where  $W_r$  is the minimum value and  $W_p$  the value reached at the plateau (see Figure 1). The activation

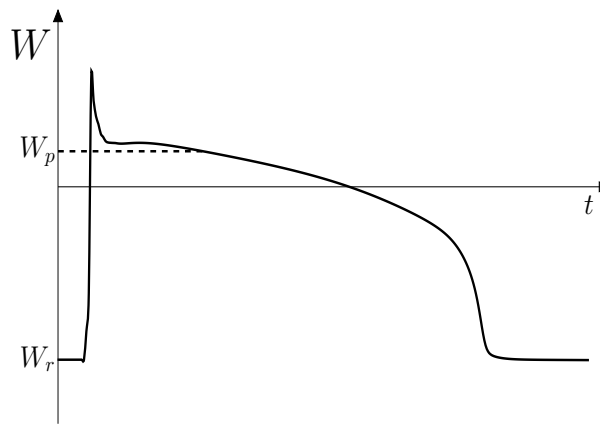


Figure 1: Characteristic waveform representing the action potential of a heart cell.

times could be obtained computationally by solving suitable mathematical models. Classical models for the mathematical description of the electrical activity in the ventricles are the *Bidomain* and the *Monodomain* models [8, 12, 23, 5], which consist in modeling the ventricular tissue as a functional syncytium of electrically coupled cells and in deriving continuous models of reaction-diffusion equations. Such models describe the electrical potential in each point of the ventricle and at each time. As a byproduct, activation times can be computed.

In this work, we decided to consider a simplified model derived from the Bidomain one, which is suitable when one needs to know only the activation times, that is the *anisotropic Eikonal equation* [11, 6]. It describes the activation time in any point of the computational domain, and it has been proved to be a good approximation of the more complex Bidomain one [6]. Such a model is far less expensive in term of computational time than the Bidomain or the Monodomain ones, since it is a steady problem and it does not exhibit an internal or boundary layer as happens when considering such models [6]. Recently, the Eikonal model has been considered also for clinical applications [20].

Let  $\Omega_m$  be the three-dimensional computational domain related to the muscular propagation and  $u_m = u_m(\mathbf{x})$  the unknown activation time. Then, the

anisotropic Eikonal model reads

$$\begin{cases} V_m \sqrt{(\nabla u_m)^T D \nabla u_m} = 1 & \mathbf{x} \in \Omega_m, \\ u_m(\mathbf{x}) = u_{m,0}(\mathbf{x}) & \mathbf{x} \in \Gamma_m, \end{cases} \quad (1)$$

where  $V_m = V_m(\mathbf{x})$  is the conduction velocity along the muscular fibers in the myocardium (possibly depending on space),  $D \in \mathbb{R}^{3 \times 3}$  is the anisotropic tensor which accounts for the orientation of the muscular fibers,  $\Gamma_m$  is the set of source points generating the front and  $u_{m,0}(\mathbf{x})$  is the value of the activation time on  $\Gamma_m$ . For the anisotropic tensor in this work we used the following expression

$$D(\mathbf{x}) = k^2 \mathbf{I} + (1 - k^2) \mathbf{a}(\mathbf{x}) \mathbf{a}(\mathbf{x})^T, \quad (2)$$

where  $k$  is the ratio between the conduction velocity orthogonal to the fibers direction and that along the fibers, and  $\mathbf{a}$  gives for each point  $\mathbf{x}$  the unit vector tangential to the fibers [6].

A more complex version of equation (1) includes also a diffusion term which accounts for the diffusion process characterizing the front (anisotropic Eikonal-Diffusion equation [6]). Such a term describes the relationship between the velocity of propagation and the curvature of the wave-front. However, as a first step in the direction of building patient-specific Purkinje networks, in this work we neglected such a contribution. The validity of such an approximation is supported by the results obtained in [22], where an excellent accuracy has been found when testing our method with real clinical data.

### 2.1.2 An approximation of the 3D problem: The isotropic Eikonal problem on the endocardium

As described later on, when the sources for the muscular activation are all located on the endocardium, then in our method for the generation of a patient-specific network it will be enough to solve a muscular problem only on the endocardium (see hypothesis H1 in Section 3). Moreover, to simplify the proposed algorithm, for the description of the electrical activity on such a surface, we considered the *isotropic* Eikonal problem. This is of course an approximation, justified by the observation that it is nowadays very hard to have information about the muscular fibers. However, as shown by the numerical experiments reported in Sections 4 and 5, this choice leads to an excellent accuracy. In particular, let  $\Omega_e$  be the computational domain related to the endocardium and  $u_e = u_e(\mathbf{x})$  the unknown activation time. Then, the isotropic 2D Eikonal model reads

$$\begin{cases} V_e |\nabla u_e| = 1 & \mathbf{x} \in \Omega_e, \\ u_e(\mathbf{x}) = u_{e,0}(\mathbf{x}) & \mathbf{x} \in \Gamma_e, \end{cases} \quad (3)$$

where  $V_e = V_e(\mathbf{x})$  is the muscular conduction velocity on the endocardium,  $\Gamma_e$  is the set of source points generating the front and  $u_{e,0}(\mathbf{x})$  is the value of the activation time on  $\Gamma_e$ .

We observe that the velocity  $V_e$  in problem (3) should be thought of as a surrogate uniform value of the anisotropic non-uniform endocardial velocity derived from  $V_m$ . In our numerical experiments  $V_e$  has been determined as the value that best agrees with the measures.

We point out that in accordance with the observations done for the 3D problem, we neglected also in this case the diffusion term.

## 2.2 The electrical activation in the Purkinje network

To solve problems (1) and (3) we need to provide the boundary conditions  $(1)_2$  and  $(3)_2$  on  $\Gamma_m$  and  $\Gamma_e$ , respectively, which represent the points where the electrical activation starts. In a normal propagation,  $\Gamma_m$  and  $\Gamma_e$  coincide with the PMJ since the signal traveling along the Purkinje network enters the muscle through these junctions. We then need a mathematical model also to describe the propagation in the Purkinje network. In this respect, it is possible to consider a one-dimensional Bidomain model as proposed in [4]. However, since we were interested in computing only the activation times in the network (in particular at the PMJ) and not the whole action potential, we considered again the Eikonal equation.

Let  $\Omega_p$  be the one-dimensional computational domain given by the Purkinje network and  $u_p = u_p(\mathbf{x})$  the unknown activation time in the network. Then, the Eikonal model reads

$$\begin{cases} V_p \left| \frac{\partial u_p}{\partial s} \right| = 1 & \mathbf{x} \in \Omega_p, \\ u_p(\mathbf{x}) = u_{p,0}(\mathbf{x}) & \mathbf{x} \in \Gamma_p, \end{cases} \quad (4)$$

where  $V_p = V_p(\mathbf{x})$  is the conduction velocity (5-10 times greater than the muscular one [13]),  $s$  is the curvilinear coordinate,  $\Gamma_p$  is the set of points generating the front (in a normal propagation  $\Gamma_p$  is the Atrioventricular node) and  $u_{p,0}(\mathbf{x})$  is the value of the activation time on  $\Gamma_p$ .

We point out that for the modelization of the network, we have considered again the isotropic Eikonal problem. This approximation is perfectly justified due to the absence of muscular fibers (and then of anisotropy) in a 1D network. Again, we neglected the diffusion term since the high advection term  $V_p$  dominates any diffusion process.

## 2.3 Numerical solution of the Eikonal problem

For the solution of the Eikonal problems (1), (3) and (4) we used algorithms belonging to the class of the *Fast Marching Methods* (FMM) [18]. Such methods are based on the observation that the information propagates only from smaller to larger values of the unknown. Based on this, FMM try to follow the front of propagation and at each step three regions are recognized:

1. The *Accepted* region, formed by the points of the domain where the solution has been already determined;
2. The *Trial* region, formed by the points of the domain “close” to the accepted ones and which are potentially new accepted points;
3. The *Far* region, formed by the points of the domain which are far from the accepted ones.

In the classical FMM, at each step of the algorithm the solution is evaluated in the trial points and a new accepted point is created. In particular, in the isotropic case, the Trial region is formed only by the points which are neighbors of the accepted ones and just a single evaluation for each trial point using an upwind scheme is enough to create a new accepted point (*single-pass method*, see [18]). In such a case, the FMM is very efficient, since it follows gradient directions, which coincide with those of propagation (*characteristic directions*). However, in the anisotropic case, the gradient and the characteristic directions do not necessarily coincide and this scheme fails to produce an accurate solution. A possible way to overcome this problem consists in enlarging the Trial region including not only the neighbors but few layers of neighbors, thus allowing the characteristic direction to remain within the neighborhood [19]. This strategy is accurate and single-pass but, in our implementations, it featured a quite high computational time. For this reason, we decided to consider in this work an alternative procedure proposed in [14], where the Trial region is formed by the neighbors solely and a recursive correction is introduced. Such a new step consists in re-computing the value of the unknown in the neighbors of each newly accepted point  $X$ , which are inside the Accepted region. This is done since when the values of the unknown has been computed in such neighbors, the value in  $X$  has not been used since it is not known. If the new evaluation in a neighbor of  $X$  returns a lower value of the unknown with respect to the previous one, then the solution in such a point is updated. This method is not anymore single-pass. However, it uses only the neighbors to compute the value of the unknown in a point, allowing for good performance from the computational point of view (see [14] for further details).

### 3 Computational generation of a patient-specific Purkinje network: The case of endocardial sources

In this section we describe the method for the generation of a patient-specific network. In particular, in this work we consider the case of sources for the muscular propagation located only on the endocardium. This is the case for example of a normal electrical propagation or of an ischemic case, where the sources are all located in the PMJ. This means that  $\Gamma_m$  in the 3D Eikonal problem and  $\Gamma_e$  in the 2D one coincide with the PMJ. In such conditions, we can consider the following two simplifying hypotheses:

- H1. For the computation of the activation times on the endocardium it is enough to solve an Eikonal problem only on the endocardium. Indeed, if the sources are all located on such a surface, the propagation in the myocardium does not have enough influence on the endocardium. Since for the generation of a patient-specific Purkinje network we only need the endocardial propagation, in our algorithm we solve only problem (3);
- H2. The propagation in the PF is not influenced by the muscular propagation, and we can assume that the information propagates uniquely from the Purkinje network towards the muscle cells and that no feedbacks from the muscle are allowed. Therefore, an explicit algorithm could be considered for the numerical solution of the coupled problems (1)-(4) and (3)-(4). In other words, we firstly solved the network solely, and then we used this solution evaluated at the PMJ as sources for the computation of the muscular activation.

We are now ready to describe the method for the generation of the patient-specific Purkinje network. This is composed of two steps: in the first one we generate a *tentative network* by using a fractal law (Section 3.1). In the second step, we update such a network in order to reduce the discrepancy with the clinical measures (Section 3.2).

We give here a description of the structure of a Purkinje network. This is formed by several levels of generation, at each of them we can identify the *active branches* and the *leaves*  $S_j$ . An active branch can generate other branches, whereas leaves, starting from the points  $\mathbf{w}_j$ , terminate at their end points  $\mathbf{y}_j$  which are identified with the PMJ  $P_j$ , see Figure 2.

### 3.1 Generation of the tentative network

The first tract of the Purkinje network is composed by the *bundle of His*, which starts from the Atrio-ventricular node, and by the *main bundle branches*, which are three branches generating from the bundle of His. The starting point of our algorithm consists in manually design the bundle of His and the main bundle branches, accordingly to anatomical a priori knowledge [1, 16]. Then, the tentative Purkinje network is generated as a fractal tree. The growing process follows the 'Y' production rule, similar to the one proposed in [1, 10, 16]. We allow the leaves to be generated after a different number of levels. However, we fix a maximum number of levels of the tree,  $M_{lev}$ , tuned in order to have a good covering of all the reachable areas of the endocardium (see Figure 2).

To ensure a correct distribution of the PMJ on the endocardium, the process of generation of a leaf is governed by a Bernoullian probability law, where the probability to generate a leaf  $p$  is a function of the tree level. In particular, we set  $p = \sqrt{j/M_{lev}}$ , where  $j$  is the current level, so that  $p$  is small for the first levels and grows in the successive levels. To obtain a more realistic pattern of PF, the

lengths of the left branch  $L_l$  and of the right branch  $L_r$ , and the branching angle  $\alpha$  of the new fibers are described by Gaussian variables.

This procedure allows to generate a tentative Purkinje network  $\mathcal{N}^{(t)}$ , characterized by  $M^{(t)}$  leaves  $S_k$  whose bases are located in  $\mathbf{w}_k$ ,  $k = 1, \dots, M^{(t)}$ , and by the PMJ  $P_k$ ,  $k = 1, \dots, M^{(t)}$ , located at the points with coordinates  $\{\mathbf{y}_1^{(t)}, \dots, \mathbf{y}_{M^{(t)}}^{(t)}\} =: \mathcal{P}^{(t)}$ , see Figure 2

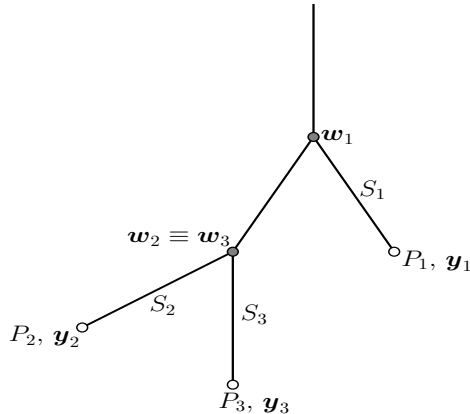


Figure 2: Structure of the Purkinje network. The grey points are the bases  $\mathbf{w}_k$  of the leaves  $S_k$ , whereas the white points represents the PMJ  $P_k$ . In the picture we have  $M_{lev} = 2$  and  $M = 3$ .

Observe that we have not yet used the clinical data, so that this is not a patient-specific network.

### 3.2 Generation of the patient-specific network

We describe here the steps to generate a patient-specific network starting from the tentative one  $\mathcal{N}^{(t)}$ , using clinical measures related to a propagation characterized by endocardial sources solely. Such data are measured on the endocardium, for example before an ablation procedure to burn anomalous propagation sites. This is possible thanks to suitable systems (such as Ensite NavX system, see, e.g., [22]), commonly used nowadays in the clinical practice, which are capable of accurately locating some electrode catheters in the ventricle, allowing for the reconstruction of a map of the activation times [17, 20].

In what follows, let  $\mathbf{x}_i$ ,  $i = 1, \dots, N$ , be the points where the measures have been acquired and  $T_i$  the related measured activation times. We summarize the steps related to the generation of the patient-specific network as follows.

**Computation of the activation times at the PMJ of  $\mathcal{N}^{(t)}$ .** We solve the 1D Eikonal problem (4) in the tentative network  $\mathcal{N}^{(t)}$ , by choosing properly the set  $\Gamma_p$  and the boundary condition  $u_{p,0}$ . For example, for a normal propagation,  $\Gamma_p$  is identified with the Atrioventricular node. This allows to compute

the activation times for all the points of  $\mathcal{N}^{(t)}$ , and in particular to store the activation times  $\tau_k^{(t)} := u_p(\mathbf{y}_k^{(t)})$ ,  $k = 1, \dots, M^{(t)}$ , computed at the PMJ.

**Construction of the regions of influence.** Ideally, the PMJ should be able to describe exactly the observed activation times. In this respect, we say that a set of  $M$  sources  $(\mathbf{z}_k, \zeta_k)$  is *compatible* with the measurements if the following holds:

$$u_e(\mathbf{x}_i) = T_i \quad \forall i = 1, \dots, N, \quad (5)$$

with

$$\begin{cases} V_e |\nabla u_e(\mathbf{x})| = 1 & \mathbf{x} \in \Omega_e, \\ u_e(\mathbf{z}_k) = \zeta_k & k = 1, \dots, M. \end{cases} \quad (6)$$

Notice that, in view of hypotheses H1, we considered the fronts propagating only on the endocardium, thus satisfying the 2D Eikonal problem (3).

To identify such compatible sources, we consider the following *backward Eikonal problem* in the unknown  $\tilde{u}_e$ :

$$\begin{cases} V_e |\nabla \tilde{u}_e(\mathbf{x})| = 1 & \mathbf{x} \in \Omega_e, \\ \tilde{u}_e(\mathbf{x}_i) = -T_i & i = 1, \dots, N. \end{cases} \quad (7)$$

The solution of such a problem divides the domain  $\Omega_e$  in  $N$  regions  $R_i$ , called *regions of influence*, which associate to any point  $\mathbf{x}_i$  the points of the endocardium which could activate  $\mathbf{x}_i$  at time  $T_i$  if used as source points for the muscular propagation. In particular, the boundaries of the regions  $R_i$  are identified by the points of collision of two or more fronts propagating from the measures' points  $\mathbf{x}_i$ . (see Figure 3 for the case  $N = 3$ ).

Exploiting the function  $\tilde{u}_e$ , we are now able to build a set of  $M$  sources that are compatible with the measures. Indeed, let  $\mathcal{Z} = \{\hat{\mathbf{z}}_1, \dots, \hat{\mathbf{z}}_M\}$  be a set of  $M$  points such that at least one point falls in each region  $R_i$  or its boundary, and  $\mathcal{Z}_i := \{\hat{\mathbf{z}}_1^i, \dots, \hat{\mathbf{z}}_{M_i}^i\}$  be the subset of points falling in  $R_i$ . Moreover, set

$$\hat{\zeta}_k := -\tilde{u}_e(\hat{\mathbf{z}}_k), \quad k = 1, \dots, M, \quad \hat{\zeta}_j^i := -\tilde{u}_e(\hat{\mathbf{z}}_j^i), \quad j = 1, \dots, M_i, \quad \forall i. \quad (8)$$

We have the following result.

**Proposition 1** *The  $M$  sources  $(\hat{\mathbf{z}}_k, \hat{\zeta}_k)$ ,  $k = 1, \dots, M$ , defined by (7)-(8) and by  $\mathcal{Z}$ , are compatible with the measures  $(\mathbf{x}_i, T_i)$ ,  $i = 1, \dots, N$ , i.e. they satisfy (5)-(6).*

**Proof.** Given some couples  $(\mathbf{z}_k, \zeta_k)$ ,  $k = 1, \dots, M$ , the solution in a point  $\mathbf{x}$  of problem (6) is given by

$$u_e(\mathbf{x}) = \min_{l=1, \dots, M} \left( \zeta_l + \frac{d(\mathbf{x}, \mathbf{z}_l)}{V_e} \right), \quad (9)$$

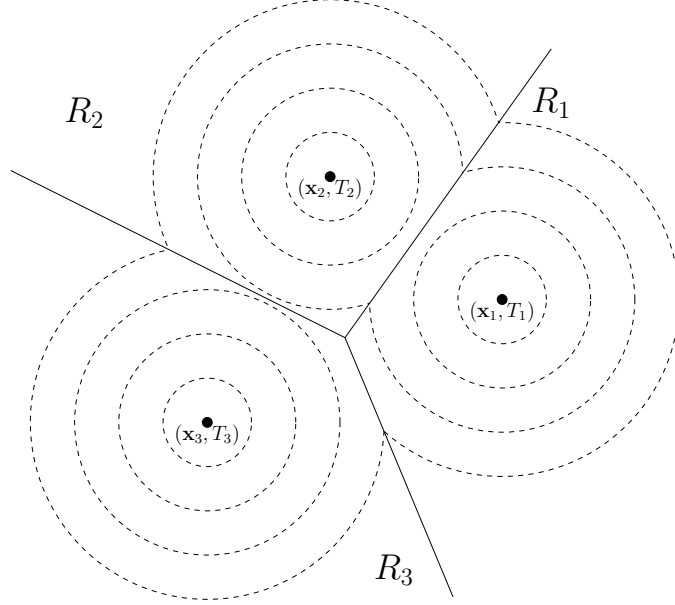


Figure 3: Regions of influence. Representation of the contour lines of a possible solution of (7) with  $N = 3$ . The lines represent the points of collision among two or more fronts, and they divide the domain in 3 regions  $R_i$ , called regions of influence.

where with  $d(\cdot, \mathbf{y})$  we have indicated the geodesic distance from  $\mathbf{y}$ . Then, constraints (5) could be written as follows

$$\min_{l=1, \dots, M} \left( \zeta_l + \frac{d(\mathbf{x}_i, \mathbf{z}_l)}{V_e} \right) = T_i \quad i = 1, \dots, N. \quad (10)$$

Analogously, the solution of problem (7) in a point  $\mathbf{x}$  is given by

$$\tilde{u}_e(\mathbf{x}) = \min_{m=1, \dots, N} \left( -T_m + \frac{d(\mathbf{x}, \mathbf{x}_m)}{V_e} \right), \quad (11)$$

and then (8) becomes

$$\hat{\zeta}_k = - \min_{m=1, \dots, N} \left( -T_m + \frac{d(\hat{\mathbf{z}}_k, \mathbf{x}_m)}{V_e} \right), \quad k = 1, \dots, M.$$

In particular, for  $\mathbf{x} \in R_i$ , the expression of (11) is simplified as follows

$$\tilde{u}_e(\mathbf{x}) = -T_i + \frac{d(\mathbf{x}, \mathbf{x}_i)}{V_e}. \quad (12)$$

Now, observing that  $\hat{\mathbf{z}}_j^i \in R_i$ , we have from (12) and (8)

$$\hat{\zeta}_j^i = - \left( -T_i + \frac{d(\hat{\mathbf{z}}_j^i, \mathbf{x}_i)}{V_e} \right), \quad j = 1 \dots, M_i. \quad (13)$$

Then, conditions (10) could be written as follows

$$\min_{m=1,\dots,N} \left( \min_{p=1,\dots,M_m} \left( \zeta_p^m + \frac{d(\mathbf{x}_i, \mathbf{z}_p^m)}{V_e} \right) \right) = T_i \quad i = 1, \dots, N,$$

where  $\zeta_j^m$  and  $\mathbf{z}_j^m$  refer to the reordering of  $\zeta_k$  and  $\mathbf{z}_k$  following the regions of influence. Then, substituting (13) in the left hand side of the previous expression, we obtain

$$\begin{aligned} & \min_{m=1,\dots,N} \left( \min_{p=1,\dots,M_m} \left( \hat{\zeta}_p^m + \frac{d(\mathbf{x}_i, \hat{\mathbf{z}}_p^m)}{V_e} \right) \right) = \\ & = \min_{m=1,\dots,N} \left( \min_{p=1,\dots,M_m} \left( T_m - \frac{d(\hat{\mathbf{z}}_p^m, \mathbf{x}_m)}{V_e} + \frac{d(\mathbf{x}_i, \hat{\mathbf{z}}_p^m)}{V_e} \right) \right) = \\ & = \min_{m=1,\dots,N} \left( \min_{p=1,\dots,M_m} \left( T_m - \frac{d(\hat{\mathbf{z}}_p^m, \mathbf{x}_m)}{V_e} + \frac{d(\mathbf{x}_i, \hat{\mathbf{z}}_p^m)}{V_e} - T_i + T_i \right) \right) = \\ & = \min_{m=1,\dots,N} \left( \min_{p=1,\dots,M_m} \left( -T_i + \frac{d(\mathbf{x}_i, \hat{\mathbf{z}}_p^m)}{V_e} - \left( -T_m + \frac{d(\hat{\mathbf{z}}_p^m, \mathbf{x}_m)}{V_e} \right) \right) \right) + T_i = T_i \quad i = 1, \dots, N, \end{aligned}$$

where the latter equality holds by noticing that the external minimum is attained for  $m = i$ , since  $-T_m + \frac{d(\hat{\mathbf{z}}_p^m, \mathbf{x}_m)}{V_e} < -T_i + \frac{d(\mathbf{x}_i, \hat{\mathbf{z}}_p^m)}{V_e}$  for  $m \neq i$  thanks to the analytical solution (12) of the backward problem and to the definition of regions of influence. Therefore, constraints (5) are satisfied and the thesis holds.  $\square$

**Improving the accuracy of the tentative network.** Once we have defined the regions of influence  $R_i$ , we can identify those of the tentative PMJ belonging to  $R_i$ , see Figure 4. In particular, we introduce the subsets  $\mathcal{P}_i^{(t)} := \{\mathbf{y}_1^{(t)i}, \dots, \mathbf{y}_{M_i^{(t)}}^{(t)i}\} \subset \mathcal{P}^{(t)}$  containing the PMJ  $P_j^i$ ,  $j = 1, \dots, M_i^{(t)}$ , belonging to  $R_i$ . The idea is now to adapt the location of the PMJ of the tentative network so as to improve the accordance with the measures, or possibly make them compatible with the measures. The regions of influence could provide useful indications on how to adapt the PMJ location to the measurements. In particular, an optimal choice would be provided by moving the PMJ in points that satisfy the hypotheses of Proposition 1, that is identifying the coordinates of the PMJ  $\mathbf{y}_k$  with  $\hat{\mathbf{z}}_k$ , and the related activation times  $\tau_k$  with  $\hat{\zeta}_k$ . Indeed, thanks to Proposition 1 this would lead to a set of compatible sources.

Observe however, that the activation time of the PMJ cannot be chosen arbitrarily as it has to be a solution of the 1D Eikonal problem (4). Moreover, we constraint the movement of the PMJ to stay within its region of influence and to be relatively small so that the length of the modified branch is still in the physiological range. Under these constraints there is no guarantee to satisfy exactly the measures. We therefore aim at developing a strategy that improves the tentative network, still fulfilling the above constraints, reducing the discrepancy with the measures. In particular, we look for new positions  $\mathbf{y}_k$  of the PMJ and for the related activation times  $\tau_k = u_p(\mathbf{y}_k)$  in an iterative framework, that is by generating a sequence of networks.

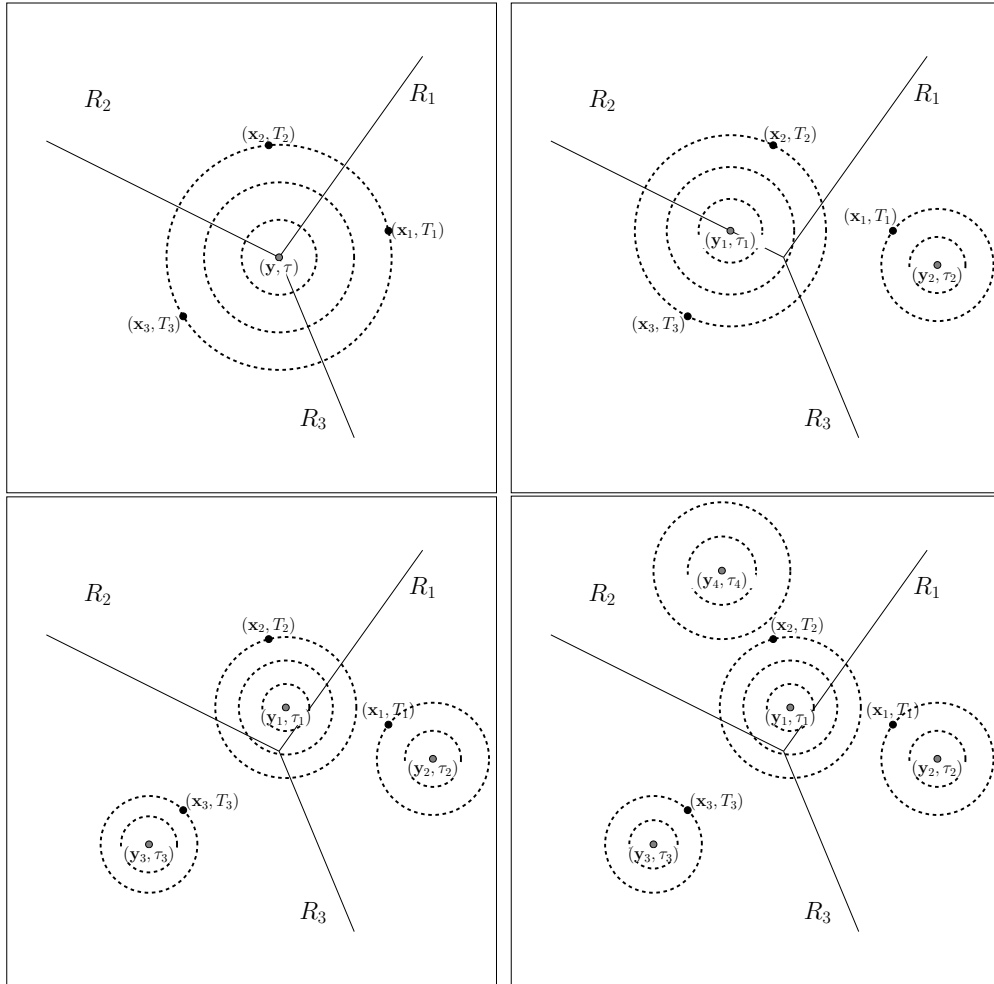


Figure 4: Examples of possible PMJ configurations. (a) Single PMJ located at the common point of the three regions of influence; (b) Two PMJ, one on the boundary between  $R_2$  e  $R_3$ , the other one in  $R_1$ ; (c) Three PMJ each one located in a different region; (d) Four PMJ, three of them,  $\mathbf{y}_1$ ,  $\mathbf{y}_2$ ,  $\mathbf{y}_3$ , which activate a measure point  $(\mathbf{x}_1, T_1)$ ,  $(\mathbf{x}_2, T_2)$ ,  $(\mathbf{x}_3, T_3)$ , respectively), and the fourth one,  $\mathbf{y}_4$ , which does not activate any measure point.

To this aim, we quantify the accuracy of a network by computing the percentage of *satisfied points*. A datum located at  $\mathbf{x}_i$  is said to be *satisfied* if

$$|\eta_i| \leq \varepsilon, \quad (14)$$

where  $\eta_i$  is given by

$$\eta_i := \frac{t_i - T_i}{|T_i|}, \quad i = 1, \dots, N, \quad (15)$$

$t_i := u_e(\mathbf{x}_i)$ ,  $i = 1, \dots, N$ , being the activation times computed at the measures' points by solving the 2D Eikonal problem (3) on the endocardium with the PMJ as boundary points (that is  $\Gamma_e = \{\mathbf{y}_1, \dots, \mathbf{y}_M\}$ ) and by using the activation times  $\tau_k$  as boundary condition  $u_{e,0}$ . Here, we have exploited hypothesis H2 which allows us to use an explicit method to solve the coupled problem given by the interaction between the propagation in the network and in the muscle.

We observe, however, that to check conditions (14) one needs to solve a forward 2D Eikonal problem for each new network generated by the algorithm. To limit the number of 2D problem to solve, we decided instead to use the discrepancy between the backward 2D Eikonal solution evaluated in a PMJ and the related activation time computed by the 1D Eikonal problem on the tentative network. This has the advantage to use the solution of the backward 2D Eikonal problem, which has been already solved to identify the regions of influence.

To this aim, given a measure  $\mathbf{x}_i$ , we introduce the quantities

$$\chi_j^i := \frac{\tau_j^i - (-\tilde{u}_e(\mathbf{y}_j^i))}{|T_i|}, \quad j = 1, \dots, M_i, \quad (16)$$

that is the discrepancy between the activation time in a PMJ  $P_j^i \in \mathcal{P}_i$  obtained by solving the 1D Eikonal problem in the tentative network and the solution of the backward Eikonal problem (7) evaluated in  $P_j^i$ , normalized by the measure  $|T_i|$ , and we check that conditions

$$|\chi_j^i| \leq \varepsilon \quad (17)$$

hold for all  $i$  and  $j$ . Now, the question is whether the satisfaction of conditions (17) imply the one of conditions (14). With this respect, we have the following result, which links the behavior of the  $\eta_i$  with the one of the  $\chi_j^i$ .

**Proposition 2** *Let the following conditions hold for all the PMJ in  $\mathcal{P}$ :*

- (i)  $\mathcal{P}_i \neq \emptyset$ ,  $i = 1, \dots, N$ ;
- (ii)  $|\chi_j^i| \leq \varepsilon$   $j = 1, \dots, M_i$ , and  $i = 1, \dots, N$ ;
- (iii)  $\min_{i=1, \dots, N} \left( \min_{j=1, \dots, M_i} \chi_j^i |T_i| \right) \geq -\varepsilon T_{min}$ , where  $T_{min} := \min_{i=1, \dots, N} |T_i|$ .

*Then conditions (14) are all satisfied, that is  $|\eta_i| \leq \varepsilon$ ,  $i = 1, \dots, N$ .*

**Proof.** From the definition of  $\chi_j^i$  (16), we can write

$$\tau_j^i = -\tilde{u}_e(\mathbf{y}_j^i) + \chi_j^i |T_i|. \quad (18)$$

From (15), we have also that conditions (14) could be written as

$$T_i - \varepsilon|T_i| \leq t_i \leq T_i + \varepsilon|T_i| \quad i = 1, \dots, N. \quad (19)$$

Analogously to (11), we can write the solution of

$$\begin{cases} V_e |\nabla u_e(\mathbf{x})| = 1 & \mathbf{x} \in \Omega_e, \\ u_e(\mathbf{y}_j^i) = \tau_j^i & i = 1, \dots, N, j = 1, \dots, M_i, \end{cases}$$

as follows

$$u_e(\mathbf{x}) = \min_{m=1, \dots, N} \left( \min_{j=1, \dots, M_m} \left( \tau_j^m + \frac{d(\mathbf{x}, \mathbf{y}_j^m)}{V_e} \right) \right).$$

Then the activation time  $t_i$  at the measurement point  $\mathbf{x}_i$ , can be written as

$$t_i = u_e(\mathbf{x}_i) = \min_{m=1, \dots, N} \left( \min_{j=1, \dots, M_m} \left( \tau_j^m + \frac{d(\mathbf{x}_i, \mathbf{y}_j^m)}{V_e} \right) \right). \quad (20)$$

We fix  $i$  and we define the following quantities

$$t_j^k := \tau_j^k + \frac{d(\mathbf{x}_i, \mathbf{y}_j^k)}{V_e}, \quad k = 1, \dots, N, j = 1, \dots, M_k. \quad (21)$$

We now observe that a measure located in  $\mathbf{x}_i$  could be activated by a PMJ belonging to  $\mathcal{P}_i$  or by a PMJ not belonging to  $\mathcal{P}_i$ , so that the external minimum in (20) is fulfilled for  $m = i$  in the first case and for  $m \neq i$  in the second case. Then, from (20), in the first case we have  $t_i = t_j^i$  for some  $j = 1, \dots, M_i$ , so that conditions (19) become

$$T_i - \varepsilon|T_i| \leq \tau_j^i + \frac{d(\mathbf{x}_i, \mathbf{y}_j^i)}{V_e} \leq T_i + \varepsilon|T_i|, \quad (22)$$

which, thanks to (18) and (11), could be written as

$$T_i - \varepsilon|T_i| \leq - \min_{m=1, \dots, N} \left( -T_m + \frac{d(\mathbf{y}_j^i, \mathbf{x}_m)}{V_e} \right) + \chi_j^i |T_i| + \frac{d(\mathbf{x}_i, \mathbf{y}_j^i)}{V_e} \leq T_i + \varepsilon|T_i|.$$

Since  $\mathbf{y}_j^i \in R_i$ , then the minimum in the above inequalities is attained again for  $m = i$ , so that conditions (19) (and then conditions (14)) become

$$-\varepsilon|T_i| \leq -\frac{d(\mathbf{y}_j^i, \mathbf{x}_i)}{V_e} + \chi_j^i |T_i| + \frac{d(\mathbf{x}_i, \mathbf{y}_j^i)}{V_e} \leq \varepsilon|T_i|,$$

which are guaranteed if hypothesis (ii) holds.

Regarding the second case, the measure located in  $\mathbf{x}_i$  is activated by a PMJ not belonging to  $\mathcal{P}_i$ , let say  $\mathbf{y}_j^k$ ,  $k \neq i$ . Therefore, by observing that inequalities (22) still hold (even if in this case they are not equivalent to conditions (14)), we have

$$t_i = t_j^k < \min_{l=1, \dots, M_i} t_l^i \leq T_i + \varepsilon|T_i|. \quad (23)$$

Moreover, since  $\mathbf{y}_j^k \in R_k$ , we have from (11)

$$-\tilde{u}_e(\mathbf{y}_j^k) = T_k - \frac{d(\mathbf{x}_k, \mathbf{y}_j^k)}{V_e} \geq T_i - \frac{d(\mathbf{x}_i, \mathbf{y}_j^k)}{V_e},$$

so that, owing to (21) and (18) we obtain

$$t_i = t_j^k = -\tilde{u}_e(\mathbf{y}_j^k) + \chi_j^k |T_k| + \frac{d(\mathbf{x}_i, \mathbf{y}_j^k)}{V_e} \geq T_i - \frac{d(\mathbf{x}_i, \mathbf{y}_j^k)}{V_e} + \chi_j^k |T_k| + \frac{d(\mathbf{x}_i, \mathbf{y}_j^k)}{V_e} = T_i + \chi_j^k |T_k|.$$

Then, using hypothesis (iii), we obtain

$$t_i \geq T_i - \varepsilon T_{min} \geq T_i - \varepsilon |T_i|,$$

which, together with (23), guarantees again that conditions (19) (and then (14)) hold true.  $\square$

**Remark 1** *The satisfaction of hypotheses (i) and (ii) in the previous Proposition provides a necessary but not sufficient condition for the fulfillment of conditions (14). Observe, however, that if we considered the absolute quantities  $\eta_i := t_i - T_i$  and  $\chi_j^i := \tau_j^i + \tilde{u}_e(\mathbf{y}_j^i)$  instead of (15) and (16), then Proposition 2 holds true even if only hypotheses (i) and (ii) were satisfied. In this case, one needs only to check that the  $R_i$  are not empty and that conditions (17) are satisfied to guarantee that all conditions (14) hold true. However, the numerical results performed with this modification, lead to less accurate patient-specific Purkinje network, so that we do not consider this case here.*

We are now ready to describe our strategy, which is based on three steps:

1. Move the PMJ;
2. Delete some PMJ;
3. Create new PMJ,

which are described in what follows.

**Move the PMJ.** This step allows to obtain a new Purkinje network  $\mathcal{N}^{(0)}$  obtained as a correction of the tentative one  $\mathcal{N}^{(t)}$  by moving some PMJ according to the measures, so to improve the percentage of satisfied measurements. In particular, for all  $j = 1, \dots, M_i^{(t)}$  such that  $|\chi_j^{(t)i}| \leq \varepsilon$ , we do nothing, that is we do not move the corresponding PMJ  $P_j^i$ . On the contrary, for all  $j$  such that  $|\chi_j^{(t)i}| > \varepsilon$ , we move the corresponding PMJ  $P_j^i$  in order to improve the accordance with the clinical measure, guaranteeing however that new locations are compatible with the Purkinje network, i.e. the new couples  $(\mathbf{y}_j^{(0)i}, \tau_j^{(0)i})$  satisfy the 1D Eikonal problem (4). The solution of this problem is not unique, so that to fix a possible solution we considered the following criterion.

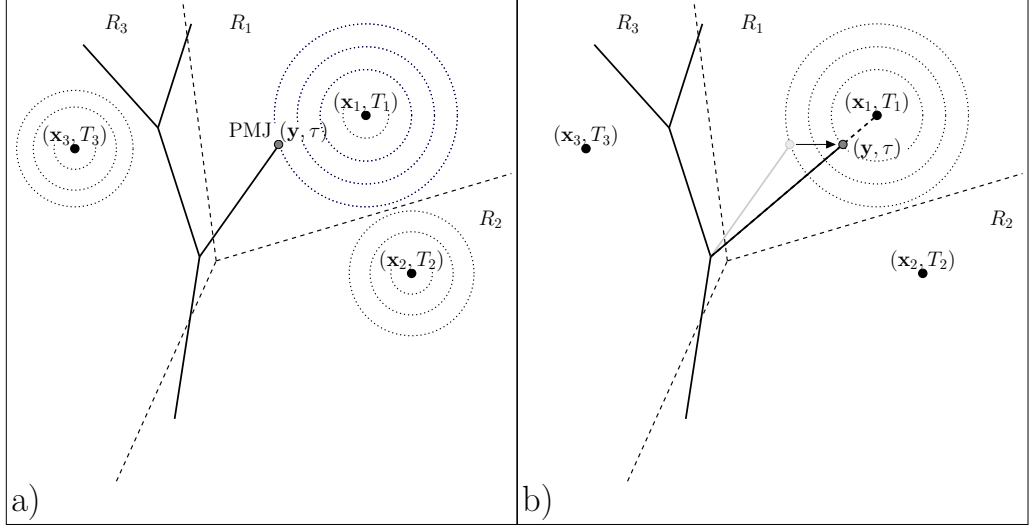


Figure 5: Moving procedure. We move the leaf and then the PMJ on the geodesic line connecting the base of the leaf with the measurement so to maximize the accordance with the measure.

**Criterion 1** *Given a non-satisfied measure  $\mathbf{x}_i$ , the PMJ  $P_j^i$  is located on the geodesic line joining the measure  $\mathbf{x}_i$  and the base of the leaf related to  $P_j^i$  (see Figure 5).*

In particular, given a point  $\mathbf{Y} = \mathbf{Y}(l)$  on the leaf  $S_j^i$  (that is the leaf corresponding to the PMJ  $P_j^i$ ), with  $l \in [l_{min}, l_{max}]$  a local (curvilinear) coordinate related to the geodesic distance, and  $l_{min}$  and  $l_{max}$  so that the length of the branch is in the physiological range, the solution of the 1D Eikonal problem (4) in  $\mathbf{Y}$  could be written as follows

$$u_p(\mathbf{Y}) = u_p^{ij}(l) := u_p(\mathbf{w}_j^i) + \frac{l}{V_p}, \quad (24)$$

where  $\mathbf{w}_j^i$  are the coordinates of the root of the leaf  $S_j^i$ . On the other side, the solution of the backward 2D Eikonal problem in  $\mathbf{Y}$  could be written as follows

$$\tilde{u}_e(\mathbf{Y}) = \tilde{u}_e^{ij}(l) := -T_i + \frac{L_j^i - l}{V_e}, \quad (25)$$

where  $L_j^i := d(\mathbf{w}_j^i, \mathbf{x}_i)$  is the geodesic distance between the measure located in  $\mathbf{x}_i$  and the base of the leaf  $S_j^i$ . Therefore, by imposing

$$u_p^{ij}(l) = -\tilde{u}_e^{ij}(l),$$

we find the distance from the base of the leaf  $S_j^i$  which guarantees that the PMJ  $P_j^i$  activates the measure located in  $\mathbf{x}_i$  and at the same time belongs to the

Purkinje network. This leads to the following optimal value

$$l_j^i = \frac{V_p V_e}{V_p - V_e} \left( u_p(\mathbf{w}_j^i) - \left( T_i - \frac{L_j^i}{V_e} \right) \right). \quad (26)$$

We then move accordingly the related PMJ, that is we set  $\mathbf{Y} = \mathbf{Y}(l_j^i)$ , guaranteeing  $\chi_j^{(0)i} = 0$  if  $l_j^i \in [l_{min}, l_{max}]$ . If  $l_j^i \notin [l_{min}, l_{max}]$ , we look for a new  $l_j^i \in [l_{min}, l_{max}]$  which minimizes  $\chi_j^i$ . Owing to (16), (24) and (25), the expression of  $\chi_j^i$  could be written as follows

$$\chi_j^i(l) = \frac{u_p^{ij}(l) + \tilde{u}_e^{ij}(l)}{|T_i|} = \frac{u_p(\mathbf{w}_j^i) - T_i + \frac{L_j^i}{V_e} + \frac{l(V_e - V_p)}{V_e V_p}}{|T_i|}, \quad j = 1, \dots, M_i.$$

Since  $V_e < V_p$ , it is easy to check that  $(\chi_j^i(l))' < 0$ , so that the minimum of  $\chi_j^i$  belongs to one of the two extrema  $l_{min}$  or  $l_{max}$ . Then, we conclude that if  $l_j^i < l_{min}$ , then we set  $l_j^i = l_{min}$ , otherwise if  $l_j^i > l_{max}$ , then we set  $l_j^i = l_{max}$ . In both the cases, we observe that we have  $\chi_j^{(0)i} \neq 0$

At the end of the moving procedure, we have obtained a new Purkinje network  $\mathcal{N}^{(0)}$  characterized by  $M^{(0)}$  PMJ. Observe that  $M^{(0)} = M^{(t)}$ .

**Delete damaging PMJ.** After the moving procedure, we have the following cases:

1.  $\chi_j^{(0)i} = 0$  for all  $j$  and  $i$ , that is all  $l_j^i$  given by (26) lie in the interval  $[l_{min}, l_{max}]$ .
2.  $\chi_j^{(0)i} \neq 0$  for some  $j$  and  $i$ , that is  $l_j^i$  given by (26) does not lie in the interval  $[l_{min}, l_{max}]$ .

In the first case, all the hypotheses of Proposition 2 are satisfied. This implies that all conditions (14) hold true, in particular it is possible to prove that  $\eta_i^{(0)} = 0$  for all  $i$ . Then, the algorithm ends and  $\mathcal{N}^{(0)}$  is the final patient-specific network.

Otherwise, in the second case Proposition 2 tells us that it could happen that  $|\eta_s^{(0)}| \geq \varepsilon$  for some  $s$  (in general we do not have necessarily  $s = i$ ), even if  $0 < |\chi_j^{(0)i}| \leq \varepsilon$ , either because some region of influence  $R_s$  could be empty (hypothesis (i) in Proposition 2 not satisfied), or because hypothesis (iii) in Proposition 2 is not satisfied. Then, we are not still guaranteeing that all conditions (14) are satisfied and we have to modify the network  $\mathcal{N}^{(0)}$ .

To this aim, we allow the algorithm to delete some PMJ and to create new ones. We firstly delete the so called ‘‘damaging’’ PMJ, that is those which avoid the satisfaction of the measures. In particular, we notice that  $|\eta_i| \geq \varepsilon$  could be given either because  $\eta_i \leq -\varepsilon$  or because  $\eta_i \geq \varepsilon$ . In the first case we do not have any chance to create a new PMJ featuring a smaller error, without deleting the

responsible of the activation in  $\mathbf{x}_i$ . Indeed, any new PMJ would be either i) in late with respect to responsible of the activation and then it could not activate  $\mathbf{x}_i$ , or ii) early, allowing then to activate  $\mathbf{x}_i$  but producing a bigger error.

In what follows we explain in the detail the delete procedure. Let  $P_q$  for some  $q = 1, \dots, M^{(0)}$ , be the PMJ which activates  $\mathbf{x}_i$ . We have to distinguish three situations:

1.  $\eta_i \leq -\varepsilon$ ,  $P_q \in \mathcal{P}_i$ . In this case, the datum in  $\mathbf{x}_i$  is activated by a PMJ belonging to  $R_i$  and the signal arrives early with respect to the measure. Then, we have not any chance to satisfy this datum since whatever movement of  $P_q$  would produce a bigger error (remember that  $P_q$  is in the optimal site with respect to Criterion 1). Moreover, we do not have any hope to satisfy the datum in  $\mathbf{x}_i$  by moving another PMJ or by creating new leaves since to produce a smaller error, the signal should be in late with respect to that produced by  $P_q$  and therefore it could not activate the point  $\mathbf{x}_i$ . Then, it is impossible to satisfy the datum in  $\mathbf{x}_i$  so that we delete PMJ  $P_q$ . This will allow if necessary to create a new PMJ which could satisfy the datum (see below);
2.  $\eta_i \leq -\varepsilon$ ,  $P_q \notin \mathcal{P}_i$ . In this case, the datum in  $\mathbf{x}_i$  is activated by  $P_q$  lying in another region of influence and the signal arrives early with respect to the measure. We can in principle move  $P_q$  to reduce the error with respect to the measure in  $\mathbf{x}_i$  since the location of  $P_q$  is not optimal with respect to  $\mathbf{x}_i$ . However, we observe that  $P_q$  could be optimal with respect to another datum  $\mathbf{x}_s$  for some  $s \neq i$ . Then, any movement of  $P_q$  lead to the loss of optimality with respect to  $\mathbf{x}_s$ , so that again we do not consider any movement of  $P_q$ . Moreover, as in the previous case, the movement of another PMJ or the generation of a new PMJ are useless to satisfy the datum  $\mathbf{x}_i$ , which is then impossible to be satisfied, and we need to delete  $P_q$ , even if with this choice the datum  $\mathbf{x}_s$  will be not in principle satisfied. However, this will allow to create new PMJ which could satisfy the two data  $\mathbf{x}_i$  and  $\mathbf{x}_s$  (see below);
3.  $\eta_i \geq \varepsilon$ . In this case, the signal is in late with respect to the measure. Then, independently of the fact that  $P_q$  belongs or not to  $\mathcal{P}_i$ , any movement of  $P_q$ , according to Criterion 1, is useless, since  $P_q$  has been located in the optimal site. However, in this case we do not need to delete  $P_q$  anymore, since this does not avoid to create new PMJ activating  $\mathbf{x}_i$ . Indeed, a new PMJ could produce a signal which is early with respect to that propagating from  $P_q$  and this allows to decrease the error. Therefore, since the presence of  $P_q$  does not avoid the generation of a new PMJ satisfying the datum, we decide to leave  $P_q$  in its original position.

Thanks to this classification, we can now describe the delete procedure. In

particular, we introduce iterations until the following criterion is satisfied

$$\eta_i^{(l)} \geq -\varepsilon \quad \forall i = 1, \dots, N. \quad (27)$$

At each iteration  $l$ , we first compute the activation times  $\tau_k^{(l)}$  in all the  $P_k$ . These values could be obtained owing to (24), thus avoiding the solution of the 1D Eikonal problem (4). We then solve the 2D Eikonal problem (3) on the endocardium by using the PMJ of  $\mathcal{N}^{(l)}$  as boundary points (that is  $\Gamma_e = \{\mathbf{y}_1^{(l)}, \dots, \mathbf{y}_{M^{(l)}}^{(l)}\}$ ) and by using the new activation times  $\tau_k^{(l)}$  as boundary condition  $u_{e,0}^{(l)}$ . This allows to obtain the new computed activation times  $t_i^{(l)}$ ,  $i = 1, \dots, N$ , at the measures' points, to compute the new values of the discrepancies  $\eta_i^{(l)}$  owing to (15), and then to identify the points  $\mathbf{x}_i$  such that (27) is not satisfied. For each of such points, we delete accordingly the PMJ responsible for its activation, so that a new network  $\mathcal{N}^{(l+1)}$  is obtained.

We observe that this procedure terminates in a finite number of iterations, let say  $K$ , allowing to produce the network  $\mathcal{N}^{(K)}$  with a positive number of PMJ.

**Remark 2** *Notice that in the delete procedure we have to solve a 2D Eikonal problem at each iteration. Observe, however, that the number of iterations in such a step is very small with respect to the one we would have in the moving procedure if we checked conditions (14) instead of (17).*

**Create new PMJ.** At the end of the *delete* procedure we are not guaranteeing that all conditions (14) are satisfied. Indeed, for some  $\mathbf{x}_i$  we could have  $\eta_i^{(K)} \geq \varepsilon$ . In this case, we consider the part of  $\mathcal{N}^{(K)}$  belonging to  $R_i$ . We select a point  $\mathbf{w}_{M_i^{(K)}+1}^i$  on such a portion of the network and we create a new leaf  $S_{M_i^{(K)}+1}^i$  lying on the geodesic line joining this point and  $\mathbf{x}_i$ . We then compute the optimal location  $l_{M_i^{(K)}+1}^i$  given by (26). If  $l_{M_i^{(K)}+1}^i \in [l_{min}, l_{max}]$ , then we leave the new PMJ in such a position which guarantees  $\chi_{M_i^{(K+1)}}^{(K+1)i} = 0$ . We observe that in this case we can infer that  $\eta_i^{(K+1)} = 0$ , since the other PMJ, thanks to the delete procedure, generate fronts which arrive in any case in late, so that they can not influence the activation in  $\mathbf{x}_i$ . If  $l_{M_i^{(K)}+1}^i \notin [l_{min}, l_{max}]$ , we then delete such a leaf and we repeat this procedure by considering another point  $\mathbf{w}_{M_i^{(K)}+1}^i$ . At the end of such a procedure we will have obtained our final network  $\mathcal{N}^{(K+1)}$  which allowed to obtain a better accuracy with respect to the tentative network.

The overall algorithm is presented in the following box.

---

**Algorithm 1** *Generation of patient-specific Pukinje network - Endocardial sources.*

---

Given the vector of the measures  $T$  in the points defined by the vector  $X$ , the conduction velocities  $V_p$  and  $V_e$ , the extrema  $L_{\min}$  and  $L_{\max}$ , the tolerance  $EPS$ , the tentative network  $NET$  and in particular the position of the PMJ  $Y$ , perform the following steps

```
Solve the 1D Eikonal problem (4) in  $NET$ ;  
Solve the backward Eikonal problem (7);  
Define the regions of influence  $R_i$ ;  
FOR  $i=1:N$   
  FOR  $j=1:M_i$   
    Compute the optimal location  $L$  with (20);  
    IF ( $L < L_{\min}$ ) THEN  $L = L_{\min}$ ;  
    ELSEIF ( $L > L_{\max}$ ) THEN  $L = L_{\max}$ ;  
    END IF  
    Move the PMJ:  $Y[i,j] \rightarrow Y[i,j]$  with (21);  
     $NET \rightarrow NET$ ;  
  END FOR  
END FOR  
Solve the Eikonal problem (3) with  $NET$  as sources;  
Compute the errors  $ETA$  with (16);  
Build the vector  $Z$  containing the PMJ activating  $X$ ;  
WHILE ( $\text{MIN}(ETA) < -EPS$ ) DO  
  FOR  $i=1:N$   
    IF ( $ETA[i] < -EPS$ ) THEN Delete  $Z[i]$ ;  
     $NET \rightarrow NET$ ;  
  END IF  
END FOR  
Solve the Eikonal problem (3) with  $NET$  as sources;  
Compute the errors  $ETA$  with (16);  
Build the vector  $Z$  containing the PMJ activating  $X$ ;  
END WHILE  
FOR  $i=1:N$   
  IF ( $ETA[i] > EPS$ ) THEN Create a new leaf owing to (20)-(21);  
END FOR
```

---

**Remark 3** *We observe that in principle our algorithm is not able to produce a network such that  $|\eta_i| \leq \varepsilon, \forall i$ . Indeed, in the create procedure the part of  $\mathcal{N}^{(K)}$  belonging to  $R_i$  could be empty for some  $i$ . In this case we do not have any chance to satisfy the datum  $\mathbf{x}_i$ .*

## 4 Numerical results in an idealized geometry

In this section we present several numerical results performed to test the reliability and the robustness of the proposed method for the generation of a patient-specific Purkinje network. To this aim we consider an idealized ventricular geometry given by the ellipsoidal model described in [7], characterized by a set of packed ellipsoidal surfaces, where the length of the semi-principal axes of the inner and outer ellipsoid are  $a_x = a_y = 1.5$  cm,  $a_z = 4.4$  cm and  $b_x = b_y = 2.7$  cm,  $b_z = 5$  cm, respectively (see Figure 6, up-left). To define the anisotropic tensor  $D$  by (2), we used the unit vectors tangent to the fibers proposed in [7], and we set  $k = 0.46$ . The resulting mesh is composed of about  $4 \cdot 10^6$  tetraedra and  $6.4 \cdot 10^5$  vertices, see Figure 6, up-right. The corresponding endocardial triangular mesh is composed of about  $1.45 \cdot 10^5$  elements and  $7.3 \cdot 10^4$  vertices.

In all the cases we used synthetic data to drive the generation of the network, obtained by solving the forward 3D problem (1) with a reference Purkinje network, see Figure 6, bottom-left. The synthetic data  $\mathcal{S} := \{(\mathbf{x}_1, T_1), \dots, (\mathbf{x}_N, T_N)\}$  were then created by sampling  $N$  points on the endocardium of the ellipsoid (see Figure 6, bottom-right). The reference network has been always built with the same procedure used to generate a tentative network. Once the patient-specific network has been generated, we assessed its accuracy by comparing the activation times obtained by solving the 3D problem (1) with the PMJ of such a network as sources, with the values of the clinical measures and those obtained by using the tentative network considered at the begin of the algorithm. In particular, we computed the mean absolute error  $E := \frac{1}{N} \sum_{i=1}^N |t_i - T_i|$  and the standard deviation  $\sigma := \sqrt{\frac{1}{N} \sum_{i=1}^N |t_i - T_i|^2 - E^2}$ .

Since the proposed method is valid only for endocardial sources (see hypotheses H1 and H2) we considered here only normal propagations where the unique source for the network was the Atrioventricular node and the unique sources for the muscle were the PMJ. In all the numerical tests of this section, unless explicitly stated otherwise, we set  $M_{lev} = 30$ ,  $V_p = 3.4$  m/s,  $V_m = 0.65$  m/s,  $\varepsilon = 10\%$ ,  $l_{min} = h$ , with  $h$  the space discretization parameter,  $l_{max} = l_{j,max}^i = \min\{0.525; L_j^i\}$ ,  $L_r L_l \sim \mathcal{G}(0.35 \text{ cm}, 0.01 \text{ cm})$ ,  $\alpha \sim \mathcal{G}(60^\circ, 1.8^\circ)$ , where  $\mathcal{G}(\mu, \sigma)$  is a Gaussian distribution with mean  $\mu$  and standard deviation  $\sigma$ . Regarding the conduction velocity on the endocardium  $V_e$  in problem (3), we have chosen every time its value by hand so to maximize the accordance with the measures.

### 4.1 Consistency test

This test has been proposed to prove the ability of our method to generate an accurate Purkinje network. In particular, we considered a sample  $\mathcal{S}$  composed by  $N = 150$  measurements well-distributed on the endocardium. We notice that the starting point of our algorithm is the tentative network, which

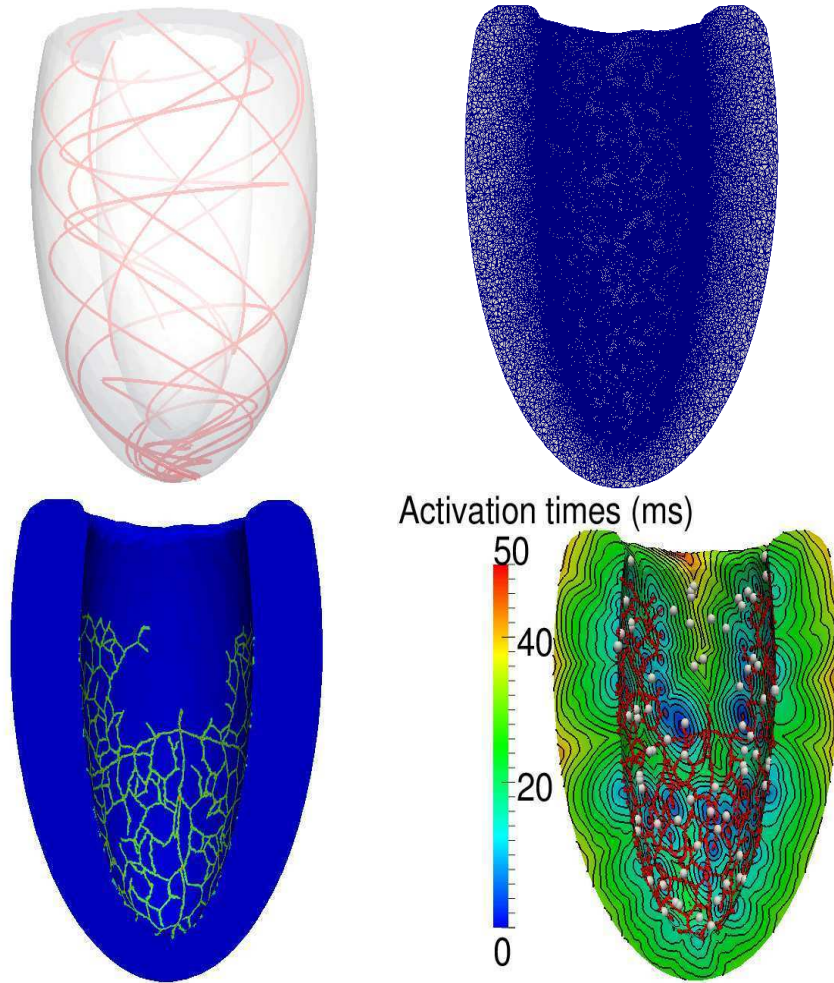


Figure 6: Procedure for the generation of the synthetic data. Up-left: Reconstructed geometry and muscular fibers; Up-right: Mesh discretization. Bottom-left: Purkinje network used in the generation of the synthetic data; Bottom-right: Activation maps obtained by solving the 3D Eikonal problem (1). The sample  $\mathcal{S}$  is represented by grey dots.

is generated randomly according to the Gaussian variables describing the length and the angle of the branches and to the Bernoullian variable describing the probability to generate a PMJ, see Section 3.1. Therefore, a consistency test should prove also the robustness of the method with respect to the tentative network and assess the variability of the results due to the randomness in the generation of the tentative network. To do this, we ran 20 times our algorithm using the same synthetic data but different (randomly generated) tentative networks. Accordingly, to assess the accuracy of the method, we have reported the average over the 20 simulations of the mean absolute er-

rors  $E^j := \frac{1}{N} \sum_{i=1}^N |t_i^j - T_i|$ ,  $j = 1, \dots, 20$ , namely  $\widehat{E} := \frac{1}{20} \sum_{j=1}^{20} E^j$ , where  $t_i^j$  is the computed activation time at point  $\mathbf{x}_i$  for the  $j$ -th numerical experiment. Regarding the standard deviation, we have to separate the spatial variability from that produced by the repetition of the experiment. In particular, the *mean spatial standard deviation* is defined by  $\sigma_{sp} := \frac{1}{20} \sum_{j=1}^{20} \sigma^j$ , where  $\sigma^j = \sqrt{\frac{1}{N} \sum_{i=1}^N |t_i^j - T_i|^2 - (E^j)^2}$  is the spatial standard deviation related to the  $j$ -th experiment, whereas the *mean standard deviation over the experiments* is given by  $\Sigma := \frac{1}{N} \sum_{i=1}^N \Sigma_i$ , where  $\Sigma_i := \sqrt{\frac{1}{20} \sum_{j=1}^{20} |t_i^j - T_i|^2 - (E_i)^2}$ ,  $E_i := \frac{1}{20} \sum_{j=1}^{20} |t_i^j - T_i|$ , is the standard deviation in the point  $\mathbf{x}_i$  over the 20 numerical experiments. To quantify the total standard deviation, we also introduced the quantity  $\widehat{\sigma} := \sqrt{\frac{1}{20} \sum_{j=1}^{20} \frac{1}{N} \sum_{i=1}^N |t_i^j - T_i|^2 - \widehat{E}^2}$ . For the experiments reported in this Section we also reported the maximum absolute error averaged over the 20 simulations  $E_{max} := \frac{1}{20} \sum_{j=1}^{20} \left( \max_{i=1, \dots, N} |t_i^j - T_i| \right)$  and the corresponding standard deviation  $\sigma_{max} := \sqrt{\frac{1}{20} \sum_{j=1}^{20} \left( \max_{i=1, \dots, N} |t_i^j - T_i| \right)^2 - E_{max}^2}$ .

The best value of the conduction velocity has been found to be  $V_e = 0.36$  m/s. The mean number of PMJ were  $M^{(t)} = 134.4 \pm 7.4$  for the tentative networks, and  $M^{(K+1)} = 193.0 \pm 11.0$  for the patient-specific networks.

In Figure 7 we depicted a selected tentative network over the 20 and the corresponding patient-specific Purkinje network obtained with our method (left) and the absolute errors at the sample  $\mathcal{S}$  (right). We observed a qualitative good improvement in the accuracy obtained by using the patient-specific network with respect to that obtained with the tentative one.

In Table 1 we compared quantitatively the accuracy of the results obtained by using the patient-specific networks generated by our method with that obtained by considering the tentative networks. In both cases, we reported the mean absolute error  $\widehat{E}$  and the standard deviations. For the sake of completeness, in

Network	$\widehat{E}$	$\sigma_{sp}$	$\Sigma$	$\widehat{\sigma}$
Tentative	3.92	3.10	2.30	3.18
Patient-specific	1.76	2.26	1.47	2.30

Table 1: Mean absolute error and standard deviations (in ms) obtained by using the tentative and the patient-specific Purkinje networks. The results have to be intended as the average over the 20 simulations. Consistency test, idealized geometry.

Table 2 we reported the spatial maximum absolute error  $E_{max}$  and the related standard deviation  $\sigma_{max}$ .

From these results, we noticed a significant improvement of the accuracy obtained by using the patient-specific network with respect to the tentative one. We also observed the small standard deviations for the case of the patient-specific

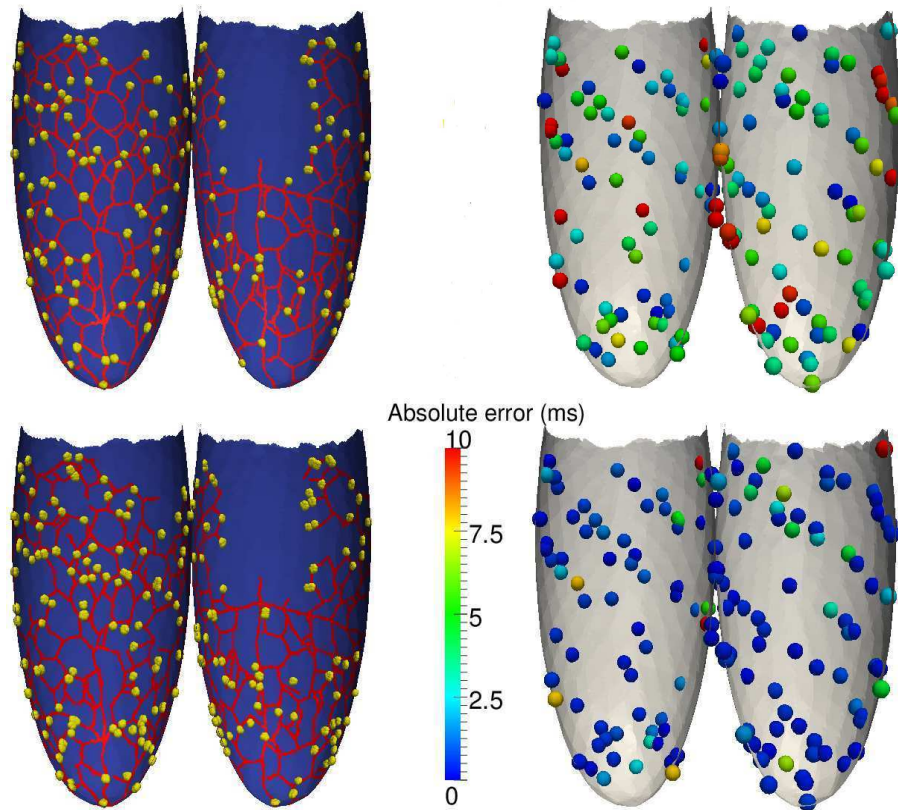


Figure 7: Left: Purkinje networks (a selected case over the 20). The PMJ are represented by the yellow spheres. Right: Absolute errors at the measures' points. Up: Tentative network. Bottom: Related patient-specific network generated by our method. Consistency test, idealized geometry.

Network	$E_{max}$	$\sigma_{max}$
Tentative	17.33	4.09
Patient-specific	12.67	3.15

Table 2: Maximum absolute error and standard deviation (in ms) obtained by using the tentative and the patient-specific Purkinje networks. The results have to be intended as the average over the 20 simulations. Consistency test, idealized geometry.

network, even smaller than those related to the tentative network. Moreover, both for the tentative and for the patient-specific network we obtained that the mean spatial standard deviation  $\sigma_{sp}$  is greater than the mean standard deviation over the experiments  $\Sigma$ . From the last two observations, we then conclude that the proposed algorithm is robust with respect to the choice of the starting network. For this reason, from now on we consider only one run of our algorithm to

generate the patient-specific network, so that we report only the global standard deviation  $\sigma$ .

**Remark 4** *As observed in Remark 3, our algorithm in principle does not guarantee that all the measures are satisfied in the sense of (14)-(15). However, we expected that the number of satisfied points should increase with respect to the tentative network. This is the case of all the numerical experiments reported in this paper. Just to provide an example, we reported in Table 3 the percentage of satisfied measures for the consistency test, showing a great improvement when passing from the tentative to the patient-specific network.*

Network	Satisfied measures (%)
Tentative	$31.1 \pm 4.1$
Patient-specific	$70.2 \pm 2.7$

Table 3: Percentage of satisfied measures obtained by using the tentative and the patient-specific Purkinje networks. The results have to be intended as the average over the 20 simulations. Consistency test, idealized geometry.

## 4.2 Cross-validation test

In this section we considered a cross-validation test, that is we divided the measures in two sets, one used to generate the patient-specific Purkinje network (the *training set*), and another one to validate the network (the *testing set*), given by the remaining points. In particular, we considered a sample  $\mathcal{S}$  of variable size  $N \geq 300$  measures well distributed and we have used a training set always composed by 300 points. The location of the measures in the training set was randomly chosen according to a uniform probability function. The best value of the conduction velocity has been found to be  $V_e = 0.36$  m/s

In Table 4 we reported the mean absolute error and the standard deviation obtained by using the patient-specific and the tentative networks for different values of  $N$ .

$N$	Tentative	Patient Specific
300	$3.74 \pm 2.83$	$1.92 \pm 2.00$
600	$3.38 \pm 2.76$	$2.75 \pm 2.64$
3000	$3.52 \pm 2.74$	$2.89 \pm 2.79$
10000	$3.63 \pm 2.84$	$2.94 \pm 2.82$

Table 4: Mean absolute error and standard deviation (in ms) obtained with respect to different testing sets. Cross-validation test, idealized geometry.

As expected, the numerical results proved that the accuracy obtained by using the tentative network were almost the same for different values of  $N$ , whereas that obtained by using the patient-specific network deteriorated for

decreasing values of measures used to generate the network. Nevertheless, the performance of the patient-specific network, even in the case when only 3% of the measures were used to drive the generation, were still superior to the tentative one. This clearly showed the improvement in the accuracy of the network when using clinical data, justifying the effort needed to generate a patient-specific network.

In the following tests, we considered all the measures to generate the patient-specific network.

### 4.3 Robustness test with respect to the samples' distribution

In this section we analyzed the robustness of the proposed method with respect to an unbalanced distributions of the synthetic data. This is the case when some regions of the endocardium are difficultly reached by the catheters or when the clinicians are interested on the activation times in a specific region. To this aim, we considered three unbalanced distributions of the synthetic data, each of them characterized by a greater density of the measures in a specific region of the endocardium. In particular, we tested the algorithm with the following samples' configurations:

- (i) Unbalanced distribution on the septum with  $N = 324$  measures (see Figure 8a);
- (ii) Unbalanced distribution on the opposite site of the septum with  $N = 366$  measures (see Figure 8b);
- (iii) Unbalanced distribution on the apex with  $N = 283$  measures (see Figure 8c).

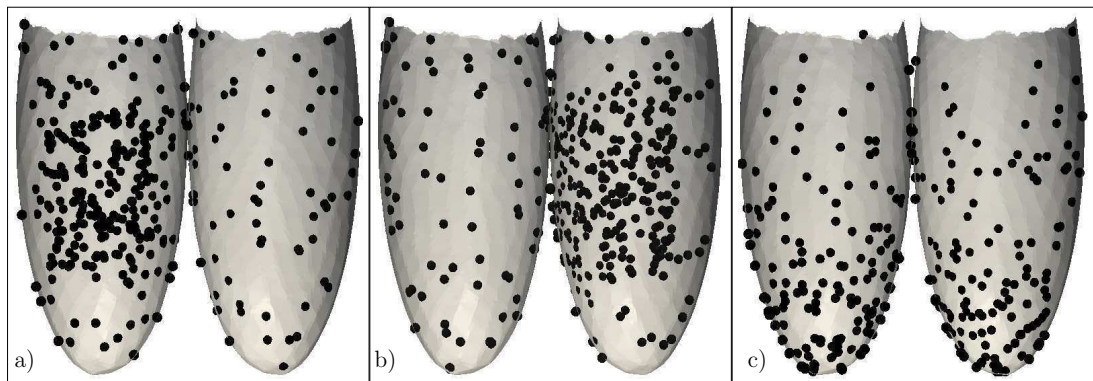


Figure 8: Representation of the unbalanced samples' distributions on the two halves of the ventricle. (a) Unbalanced distribution on the septum; (b) Unbalanced distribution on the opposite site of the septum; (c) Unbalanced distribution on the apex. Unbalanced samples' distribution, idealized geometry.

The best value of the conduction velocity has been found to be  $V_e = 0.35$  m/s for case (a) and  $V_e = 0.36$  m/s for cases (b) and (c).

In Table 5 we reported the mean absolute error and the standard deviation obtained by the patient-specific Purkinje networks generated by using the three different samples’ distributions, using the same tentative network as starting point.

Region of unbalanced measures	Tentative	Patient specific
Septum	$3.36 \pm 3.12$	$1.71 \pm 1.83$
Opposite to the septum	$3.48 \pm 2.87$	$2.07 \pm 1.95$
Apex	$4.03 \pm 2.60$	$1.92 \pm 1.86$

Table 5: Mean absolute error and standard deviation (in ms) for the patient-specific Purkinje networks generated with three different samples’ distribution and for the related tentative networks. For each row, the name indicates the region where the measures were localized. Unbalanced samples’ distribution, idealized geometry.

From these results, we found for all the cases more or less the same accuracy when using the patient-specific network. We highlight that in any case the accuracy has been increased with respect to that obtained by using the tentative network. This showed that our method should be reliable also in real cases, when the measures are not acquired uniformly, independently of the region where they are localized.

#### 4.4 Accuracy in the case of noisy data

In order to mimic the measurement error introduced by the acquisition procedure, in this section we considered synthetic data affected by noise to generate the patient-specific network. To this aim, we considered a sample of synthetic data  $\mathcal{S}$  composed by  $N = 150$  measurements well-distributed on the endocardium and we added a random noise as follows:

$$\tilde{T}_i = T_i + \omega \max_{i=1, \dots, N} \{|T_i|\} \mathcal{U}_{i[-0.5, 0.5]} \quad i = 1, \dots, N, \quad (28)$$

where  $\mathcal{U}_{i[-0.5, 0.5]}$  is the uniform probability distribution in the interval  $[-0.5, 0.5]$ , and  $\omega$  is the percentage of error. In this way, we obtained the "noisy" sample  $\tilde{\mathcal{S}}(\omega) := \{(\mathbf{x}_1, \tilde{T}_1), \dots, (\mathbf{x}_N, \tilde{T}_N)\}$  which has been then used to generate the patient-specific network. Of course, the accuracy of the generated network has been then evaluated with respect to the original sample  $\mathcal{S}$ .

In Table 6 we reported the mean absolute error and the standard deviation obtained by using the tentative and the patient-specific Purkinje network.

As expected, we found a decreased accuracy of the patient-specific network for increasing values of the noise. However, we still observed an excellent accuracy for  $\omega = 0.05$  and  $\omega = 0.1$ . In any case, the mean absolute error was better than those obtained with the tentative network, also in the case  $\omega = 0.2$ , which is probably greater to that expected by the clinical acquisition. These results

Network	$\omega$	$E \pm \sigma$
Tentative	—	$4.33 \pm 3.05$
Patient specific	0.00	$1.64 \pm 1.99$
	0.05	$1.87 \pm 2.50$
	0.10	$1.81 \pm 2.10$
	0.20	$2.42 \pm 2.35$

Table 6: Mean absolute error and standard deviation (in ms) obtained for different values of  $\omega$ . The generation of the network has been driven by the sample  $\tilde{\mathcal{S}}(\omega)$ , whilst their accuracy has been evaluated with respect to the sample  $\mathcal{S}$ . Noisy data, idealized geometry.

highlighted the robustness and accuracy of our method also in the presence of noisy data, justifying the effort needed to generate a patient-specific network.

## 5 Application to a real case

In this section we present two applications of the proposed method to a real geometry reconstructed starting from Magnetic Resonance Images (MRI): In the first one we considered real clinical data related to a normal propagation, while in the second one we generated synthetic data to simulate the presence of a myocardial ischemia. The 3D geometry has been manually segmented from the MRI data and it has been discretized in a tetrahedral mesh composed of about  $2.85 \cdot 10^5$  vertices and  $1.5 \cdot 10^6$  elements. Since we did not have any information about the muscular fibers, we assumed in any case an isotropic propagation through the myocardium, that is for the solution of (1) we set  $k = 1$  in (2) and then  $D = I$ . Then, in our algorithm we have set  $V_e = V_m$  and no optimization on  $V_e$  was in this case needed.

### 5.1 Clinical data related to a normal propagation

In the first application we considered a case characterized by a normal propagation. The related activation times on the endocardium were acquired with the EnSite NavX system, see [22] for more details. In Figure 9 we represent the patient-specific Purkinje network obtained by using all the clinical data to drive the network generation.

The accuracy of the generated patient-specific network on the endocardium has been already studied in [22], where a cross-validation test highlighted the suitability of our method for real data, see [22] for more details. Here, we wanted to study the accuracy of the solution, obtained by using the patient-specific network, in the myocardium. The conduction velocities in the network and in the myocardium have been set in order to maximize the agreement with the clinical data. In particular, we used the following values:  $V_p = 3.9$  m/s,  $V_m = V_e = 0.6$  m/s.



Figure 9: Patient-specific Purkinje network generated from clinical data related to a normal ventricular activation. The PMJ are represented by the red spheres. Normal propagation, real geometry and data.

In Figure 10 we showed the contour lines of the activation maps obtained by solving problem (1) with the patient-specific network generated by our algorithm.

Since we did not have at disposal clinical measures in the myocardium, but only on the endocardium, we provided here only qualitative observations. In particular, comparing our results with the activation maps reported in [9], we noticed that, despite neglecting the muscular fibers architecture, there was a good accordance in the overall pattern of activation. In particular, we noticed that the signal originated at the septum and ended at the base of the ventricle after about 60 ms, a value in accordance with the one reported in [9]. A quantitative validation in the myocardium would require to acquire measures also below the endocardium, a not common procedure nowadays in the clinical practice.

## 5.2 Simulating an ischemic case

As observed, our method is not only valid in the case of a normal electrical propagation. Indeed, the only requirement for its validity is that the sources for the muscular activation are all located on the endocardium. Therefore, our method is still valid for a case characterized by a normal propagation in the network, with the presence of a myocardial ischemia in the muscle, that is a region characterized by reduced blood supply, resulting in the death of the muscular cells and thus in a progressive deterioration of the electrical activity (see [24] for

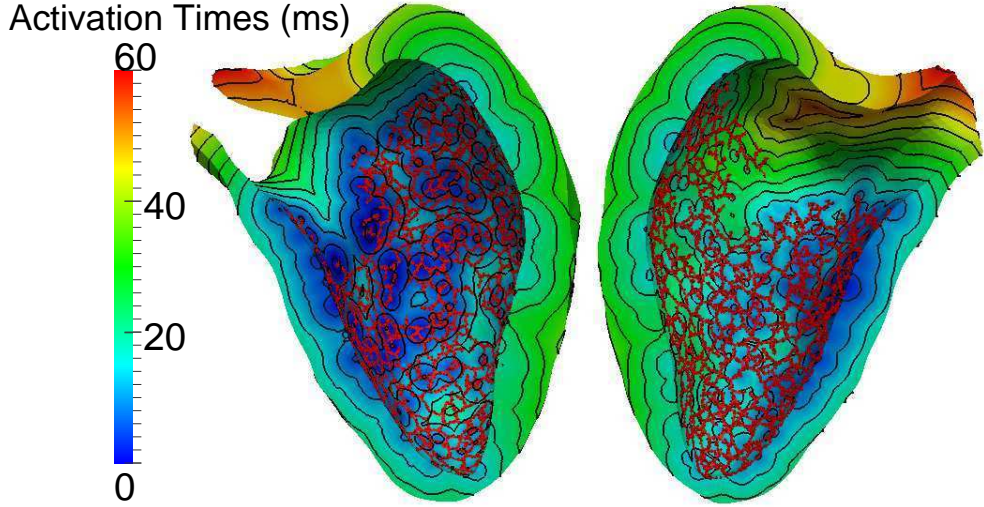


Figure 10: Activation maps obtained by solving the 3D isotropic Eikonal problem in the patient-specific geometry with the patient-specific Purkinje network generated from clinical data. Normal propagation, real geometry and data.

a computational study).

Since we did not have real clinical data for the patient at hand related to a myocardial ischemia, we generated synthetic data by solving the 3D Eikonal problem (1) with a reference Purkinje network. In the ischemic region, in what follows denoted by  $\mathcal{I}$ , we supposed that the myocardium is no longer excitable, that is we set

$$V_m(\mathbf{x}) = \begin{cases} 0.65 \text{ m/s}, & \text{if } x \notin \mathcal{I}, \\ 0.00 \text{ m/s}, & \text{if } x \in \mathcal{I}, \end{cases}$$

whereas we assumed that the portion of the Purkinje network corresponding to that region was characterized by a reduced conduction velocity, since also the cells of the network are supposed to die under the reduced blood supply. In particular, we set

$$V_p(\mathbf{x}) = \begin{cases} 3.90 \text{ m/s}, & \text{if } x \notin \mathcal{I}, \\ 0.39 \text{ m/s}, & \text{if } x \in \mathcal{I}. \end{cases} \quad (29)$$

Again, the reference network used to generate the synthetic data has been built with the same procedure used to generate a tentative network. In this way, the synthetic data  $\mathcal{S}^{\mathcal{I}} := \{(\mathbf{x}_1^{\mathcal{I}}, T_1^{\mathcal{I}}), \dots, (\mathbf{x}_N^{\mathcal{I}}, T_N^{\mathcal{I}})\}$  were obtained by sampling  $N = 150$  points on the endocardium with the exception of  $\mathcal{I}$ , since the ischemic region was not excitable.

We then apply the proposed method for the generation of the patient-specific network, supposing to know the location of the ischemic region. In Figure 11 we depicted the simulated activation maps obtained by solving problem (1) with

the generated patient-specific network, and the absolute errors at the measures' points.

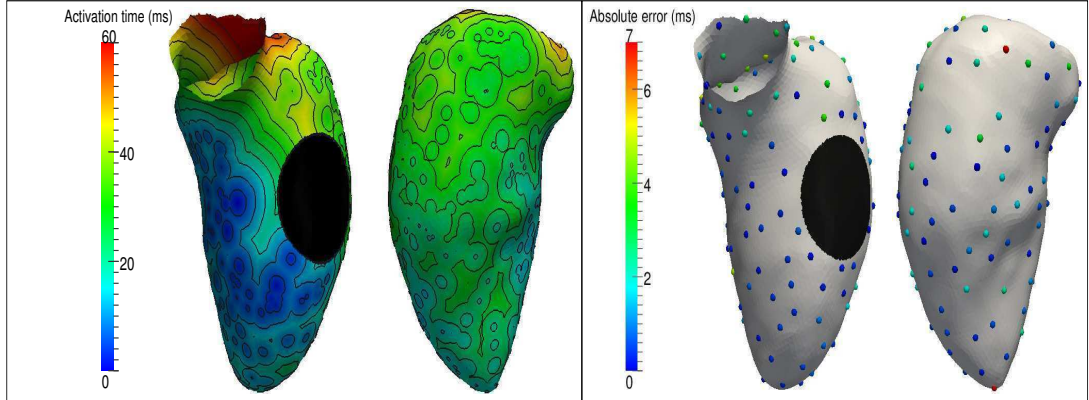


Figure 11: Left: Activation maps on the endocardium using the patient-specific Purkinje network generated by using the measures in  $\mathcal{S}^{\mathcal{I}}$ ; Right: Absolute error at the measures' points. Case with ischemia, real geometry, synthetic data.

The numerical results showed that 88.6% of the measures were satisfied when using the patient-specific network (34.0% for the tentative one), and that the mean absolute error was  $1.30 \text{ ms} \pm 1.51 \text{ ms}$  ( $3.37 \text{ ms} \pm 2.61 \text{ ms}$  for the tentative network). This consistency test proved the reliability of the proposed method in the case of the presence of an ischemic region. Of course, a validation performed with real data of such a pathology will be mandatory. This is under study and it will be the subject of future works.

## 6 Conclusions

In this work we proposed a new method for the generation of a patient-specific Purkinje network driven by clinical measures of the activation times on the endocardium. In particular, we considered the case of sources for the muscular activation all located on the endocardium, as happens, for example, for a normal electrical activity or for an ischemic case.

Our algorithm was based on the correction of a tentative network, generated by using a fractal law as proposed in [1, 10, 16], improving the accordance with the measures. Its implementation is very simple and its efficiency very high since it requires the solution of 2D isotropic Eikonal problems on the endocardium, thus avoiding the knowledge of the muscular fibers and the computation in all the myocardium.

In the case of an ideal geometry and synthetic data, our numerical results highlighted:

1. The consistency of our method and the robustness with respect to the (randomly generated) tentative network;
2. The accuracy of our method when a cross-validation test was performed;
3. The robustness of our method when unbalanced or noisy data were considered;
4. A better accuracy in all the cases with respect the one obtained with the tentative network.

Moreover, the numerical experiments performed in a real geometry highlighted:

5. The qualitative accordance of the activation maps in the myocardium obtained by using a patient-specific network generated with real data, when compared with those reported in [9];
6. The accuracy of our method when an ischemic region characterized by a vanishing conduction velocity was considered to generate synthetic data.

For all these reasons, we believe that the proposed method could be an effective tool to improve the accuracy of the numerical results in computational electrocardiology.

We point out that the accuracy of our method to real cases characterized by a normal propagation has been already discussed in [22]. Other possible perspectives will be:

- The application of our method to pathological cases with endocardial sources (such as an ischemia) by using real clinical data;
- The extension and the application of our method to cases where the muscular sources are not all located on the endocardium, such as in the Wolff-Parkinson-White syndrome;
- The extension of our method to the case where more accurate models, such as the Bidomain one, will be considered to compute the ventricular electrical activity.

## Acknowledgements

The present study has been funded by “Fondazione Cassa di Risparmio di Trento e Rovereto” (CARITRO) within the project “Numerical modelling of the electrical activity of the heart for the study of the ventricular dyssynchrony”. The authors would like to thank M. Centonze and D. Catanzariti for having provided the radiological images and the electrical activation data.

## References

- [1] S. Abboud, O. Berenfeld, and D. Sadeh. Simulation of high-resolution qrs complex using a ventricular model with a fractal conduction system. effects of ischemia on high-frequency qrs potentials. *Circ Res*, 68(6):1751–1760, 1991.
- [2] R.H. Anderson, J. Yanni, M.R. Boyett, N.J. Chandler, and H. Dobrzynski. The anatomy of the cardiac conduction system. *Clin Anat*, 22(1):99–113, 2009.
- [3] O. Berenfeld and J. Jalife. Purkinje-muscle reentry as a mechanism of polymorphic ventricular arrhythmias in a 3-dimensional model of the ventricles. *Circ Res*, 2(10):1063–1077, 1998.
- [4] R. Bordas, K. Gillow, Q. Lou, I.R. Efimov, D. Gavaghan, P. Kohl, V. Grau, and B. Rodriguez. Rabbit-specific ventricular model of cardiac electrophysiological function including specialized conduction system. *Prog Biophys Mol Biol*, 107(1):90–100, 2011.
- [5] R.H. Clayton, E.M. Cherry O. Bernus and, H. Dierckx, F.H. Fenton, L. Mirabella, A.V. Panfilov, F.B. Sachse, and G. Seemann H. Zhang. Models of cardiac tissue electrophysiology: Progress, challenges and open questions. *Progress in Biophysics and Molecular Biology*, 104(1-3):22–48, 2011.
- [6] P. Colli Franzone and L. Guerri. Spreading excitation in 3-d models of the anisotropic cardiac tissue, I. validation of the Eikonal model. *Math Biosci*, 113:145–209, 1993.
- [7] P. Colli Franzone, L. Guerri, M. Pennacchio, and B. Taccardi. Spreading excitation in 3-d models of the anisotropic cardiac tissue, II. effects of the fiber architecture and ventricular geometry. *Math Biosci*, 147:131171, 1998.
- [8] P. Colli Franzone and L.F. Pavarino. A parallel solver for reactiondiffusion systems in computational electrocardiology. *Math Models Methods Appl Sc*, 14(06):883–911, 2004.
- [9] D. Durrer, R.R. van Dam, G.E. Freud, M.J. Janse, F.L. Meijler, and R.C. Arzbaecher. Total excitation of the isolated human heart. *Circulation*, 41(6):899–912, 1970.
- [10] T. Ijiri, T. Ashihara, T. Yamaguchi, K. Takayama, T. Igarashi, T. Shimada, T. Namba, R. Haraguchi, and K. Nakazawa. A procedural method for modeling the purkinje fibers of the heart. *Prog Biophys Mol Biol*, 58(7):90–100, 2008.
- [11] J.P. Keener. An eikonal-curvature equation for action potential propagation in myocardium. *J Math Biol*, 29(7):629–651, 1991.

- [12] J.P. Keener and K. Bogar. A numerical method for the solution of the bidomain equations in cardiac tissue. *Chaos*, 8(1):234–241, 1998.
- [13] B. Kerckoffs, O.P. Faris, P.H. Boveenderd, F.W. Prinzen, K. Smits, and T. Arts. Timing of depolarization and contraction in the paced canine left ventricle:. *Journal of Cardiovascular Electrophysiology*, 14:S188–S195, 2003.
- [14] E. Konukoglu, M. Sermesant, O. Clatz, J.M. Peyrat, H. Delingette, and N. Ayache. *A recursive anisotropic fast marching approach to reaction diffusion equation: Application to tumor growth modeling*, volume IPMI 2007, LNCS 4584, pages 687–699. Springer-Verlag Berlin Heidelberg, 2007.
- [15] D.A. Rawling, R.W. Joyner, and E.D. Overholt. Variations in the functional electrical coupling between the subendocardial purkinje and ventricular layers of the canine left ventricle. *Circ Res*, 57(2):252–261, 1985.
- [16] R. Sebastian, V. Zimmerman, D. Romero, and A.F. Frangi. Construction of a computational anatomical model of the peripheral cardiac conduction system. *Prog Biophys Mol Biol*, 58(12):90–100, 2011.
- [17] M. Sermesant, R. Chabiniok, P. Chinchapatnam, T. Mansi, F. Billet, P. Moireau, J.M. Peyrat, K. Wong, J. Relan, K. Rhode, M. Ginks, P. Lambiase, H. Delingette, M. Sorine, C.A. Rinaldi, D. Chapelle, R. Razavi, and N. Ayache. Patient-specific electromechanical models of the heart for the prediction of pacing acute effects in crt: a preliminary clinical validation. *Med Image Anal*, 16(1):201–215, 2012.
- [18] J. A. Sethian. Fast marching methods. *Siam Review*, 41(2):199–235, 1999.
- [19] J. A. Sethian and A. Vladimirovsky. Ordered upwind methods for static hamilton-jacobi equations: Theory and algorithms. *Siam J Num Anal*, 41(1):325–363, 2003.
- [20] C. Tobon-Gomez, N. Duchateau, R. Sebastian, S. Marchesseau, O. Camara, E. Donal, M. De Craene, A. Pashaei, J. Relan, M. Steghofer, P. Lamata, H. Delingette, S. Duckett, M. Garreau, A. Hernandez, K.S. Rhode, M. Sermesant, N. Ayache, C. Leclercq, R. Razavi, N.P. Smith, and A.F. Frangi. Understanding the mechanisms amenable to CRT response: from pre-operative multimodal image data to patient-specific computational models. *Med Biol Eng Comput*, doi: 10.1007/s11517-013-1044-7, 2013.
- [21] K.H. Tusscher and A.V. Panfilov. Modelling of the ventricular conduction system. *Prog Biophys Mol Biol*, 96(1-3):152–170, 2008.
- [22] C. Vergara, S. Palamara, D. Catanzariti, C. Pangrazzi, F. Nobile, M. Centonze, E. Faggiano, M. Maines, A. Quarteroni, and G. Vergara. Patient-specific generation of the purkinje network driven by clinical measurements.

MOX-Report n. 09-2013, Dipartimento di Matematica, Politecnico di Milano, Italy, 2013.

- [23] E.J. Vigmond, F. Aguel, and N.A. Trayanova. Computational techniques for solving the bidomain equations in three dimensions. *IEEE Trans Biomed Eng*, 49(11):1260–1269, 2002.
- [24] D. Wang, R.M. Kirby, R.S. MacLeod, and C.R. Johnson. Inverse electrocardiographic source localization of ischemia: An optimization framework and finite element solution. *Journal of Computational Physics*, 250:403–424, 2013.

# MOX Technical Reports, last issues

Dipartimento di Matematica “F. Brioschi”,  
Politecnico di Milano, Via Bonardi 9 - 20133 Milano (Italy)

- 47/2013** CHKIFA, A.; COHEN, A.; MIGLIORATI, G.; NOBILE, F.; TEMPONE, R.  
*Discrete least squares polynomial approximation with random evaluations - application to parametric and stochastic elliptic PDEs*
- 48/2013** SIMONE PALAMARA, CHRISTIAN VERGARA, ELENA FAGGIANO, FABIO NOBILE  
*An effective algorithm for the generation of patient-specific Purkinje networks in computational electrocardiology*
- 45/2013** SANGALLI, L.M.; SECCHI, P.; VANTINI, S.  
*Analysis of AneuRisk65 data: K-mean Alignment*
- 46/2013** MARRON, J.S.; RAMSAY, J.O.; SANGALLI, L.M.; SRIVASTAVA, A.  
*Statistics of Time Warpings and Phase Variations*
- 44/2013** SANGALLI, L.M.; SECCHI, P.; VANTINI, S.  
*AneuRisk65: a dataset of three-dimensional cerebral vascular geometries*
- 43/2013** PATRIARCA, M.; SANGALLI, L.M.; SECCHI, P.; VANTINI, S.  
*Analysis of Spike Train Data: an Application of K-mean Alignment*
- 42/2013** BERNARDI, M.; SANGALLI, L.M.; SECCHI, P.; VANTINI, S.  
*Analysis of Juggling Data: an Application of K-mean Alignment*
- 41/2013** BERNARDI, M.; SANGALLI, L.M.; SECCHI, P.; VANTINI, S.  
*Analysis of Proteomics data: Block K-mean Alignment*
- 40/2013** PACCIARINI P.; ROZZA G.  
*Stabilized reduced basis method for parametrized advection-diffusion PDEs*
- 39/2013** IEVA, F.; MARRA, G.; PAGANONI, A.M.; RADICE, R.  
*A semiparametric bivariate probit model for joint modeling of outcomes in STEMI patients*